Facilitated dissociation of transcription factors from single DNA binding sites

Ramsey I. Kamar[a], Edward J. Banigan[b], Aykut Erbas[c], Rebecca D. Giuntoli[a], Monica Olvera de la Cruz[b,c,d,1], Reid C. Johnson[e], and John F. Marko[a,b,1]

[a]Department of Molecular Biosciences, Northwestern University, Evanston, IL 60208; [b]Department of Physics and Astronomy, Northwestern University, Evanston, IL 60208; [c]Department of Materials Science and Engineering, Northwestern University, Evanston, IL 60208; [d]Department of Chemistry, Northwestern University, Evanston, IL 60208; and [e]Department of Biological Chemistry, David Geffen School of Medicine at the University of California, Los Angeles, CA 90095

Contributed by Monica Olvera de la Cruz, February 14, 2017 (sent for review December 14, 2016; reviewed by Alfredo Alexander-Katz and Joseph J. Loparo)

The binding of transcription factors (TFs) to DNA controls most aspects of cellular function, making the understanding of their binding kinetics imperative. The standard description of bimolecular interactions posits that TF off rates are independent of TF concentration in solution. However, recent observations have revealed that proteins in solution can accelerate the dissociation of DNA-bound proteins. To study the molecular basis of facilitated dissociation (FD), we have used single-molecule imaging to measure dissociation kinetics of Fis, a key *Escherichia coli* TF and major bacterial nucleoid protein, from single dsDNA binding sites. We observe a strong FD effect characterized by an exchange rate $\sim 1\times 10^4$ $M^{-1}s^{-1}$, establishing that FD of Fis occurs at the single-binding site level, and we find that the off rate saturates at large Fis concentrations in solution. Although spontaneous (i.e., competitor-free) dissociation shows a strong salt dependence, we find that FD depends only weakly on salt. These results are quantitatively explained by a model in which partially dissociated bound proteins are susceptible to invasion by competitor proteins in solution. We also report FD of NHP6A, a yeast TF with structure that differs significantly from Fis. We further perform molecular dynamics simulations, which indicate that FD can occur for molecules that interact far more weakly than those that we have studied. Taken together, our results indicate that FD is a general mechanism assisting in the local removal of TFs from their binding sites and does not necessarily require cooperativity, clustering, or binding site overlap.

DNA–protein interactions | biomolecule binding | chemical kinetics | transcription factor | facilitated dissociation

Protein–DNA interactions ultimately control all aspects of cellular function through their actions as "transcription factors" (TFs) by regulating gene transcription, folding DNA into chromosomes, and modifying the structure of chromatin; these regulatory and structural functions are often interwoven (1–9). Understanding protein–DNA interaction kinetics is, therefore, essential to the mechanistic understanding of cellular function. The standard picture of protein–DNA interactions assumes binding via concentration-dependent association and concentration-independent "spontaneous dissociation" kinetics, with net affinity neatly described by the ratio of the off rate, $k_{\rm off}$, to the association rate constant, γ (i.e., $K_{\rm D}=k_{\rm off}/\gamma$). Experiments that resolve dynamics of individual molecules are starting to challenge this classical picture: lifetimes of DNA–protein complexes have been found to be appreciably shortened by nearby proteins that compete for space on DNA (10–20). However, the molecular mechanisms underlying this "facilitated dissociation" (FD) effect remain unclear.

A well-characterized DNA binding protein that has shown strong FD effects is the *Escherichia coli* TF Fis (13, 14). This dimeric TF binds diverse but sequence-specific DNA sites through a pair of helix–turn–helix domains to form a stable protein–DNA complex (21). Fis also has a weaker, but appreciable, nonsequence-specific DNA binding affinity that contributes to its role as a chromosome-organizing protein (22). This previous body of work establishes the Fis–DNA complex as a model system for studying the molecular basis of FD.

In this paper, we present single-molecule experiments on the Fis–DNA system plus theoretical analyses that establish that, through FD, competitor proteins can strongly modulate the stability of a single-protein dimer bound to a single DNA binding site, leading to a concentration-dependent off rate. The off rate saturates at high protein concentration, indicating the presence of a rate-limiting step along the FD pathway. Our experiments establish that FD can occur at the single-binding site level without the need for cooperative effects via clusters of multiple proteins or long segments of DNA (13). We also find that spontaneous dissociation and FD have distinct dependences on salt concentration. Our data for Fis are globally and quantitatively described by an analytically tractable theory, in which FD is generated by partial dissociation of the initially bound Fis, thereby allowing an unstable Fis–DNA–Fis ternary complex to form (10, 11, 13, 16, 18–20, 23–28). We validate our analytical theory using molecular dynamics (MD) simulations of FD that explicitly incorporate ionic effects. Finally, additional experimental data for a monomeric yeast TF, NHP6A, which binds a different short DNA through a single HMG box interaction (9), also display FD, indicating that the two DNA binding domains of Fis are not required for a protein–DNA complex to display concentration-dependent dissociation kinetics. Based on our results, we expect FD to be a generic effect that modulates the effective affinity of TF–DNA interactions in cells.

Significance

Transcription factors (TFs) control biological processes by binding and unbinding to DNA. Therefore, it is crucial to understand the mechanisms that affect TF binding kinetics. Recent studies challenge the standard picture of TF binding kinetics by showing cases of proteins in solution accelerating TF dissociation rates through a facilitated dissociation (FD) process. Our study shows that FD can occur at the level of single binding sites without the action of large protein clusters or long DNA segments. Our results quantitatively support a model of FD in which competitor proteins invade partially dissociated states of DNA-bound TFs. FD is expected to be a general mechanism for modulating gene expression by altering the occupancy of TFs on the genome.

Author contributions: R.I.K., E.J.B., A.E., R.D.G., M.O.d.l.C., R.C.J., and J.F.M. designed research; R.I.K., E.J.B., A.E., R.D.G., M.O.d.l.C., R.C.J., and J.F.M. performed research; R.I.K., E.J.B., A.E., R.D.G., R.C.J., and J.F.M. contributed new reagents/analytic tools; R.I.K., E.J.B., A.E., R.D.G., R.C.J., and J.F.M. analyzed data; and R.I.K., E.J.B., A.E., R.D.G., M.O.d.l.C., R.C.J., and J.F.M. wrote the paper.

Reviewers: A.A.-K., Massachusetts Institute of Technology; and J.J.L., Harvard Medical School.

The authors declare no conflict of interest.

[1]To whom correspondence may be addressed. Email: m-olvera@northwestern.edu or john-marko@northwestern.edu.

This article contains supporting information online at www.pnas.org/lookup/suppl/doi:10.1073/pnas.1701884114/-/DCSupplemental.

Results

Fis Stably Binds a Short Minimal Binding Sequence. We used single-molecule fluorescence imaging to measure the dissociation kinetics of gfpFis from individual DNA binding sites (Fig. 1). We immobilized one end of 27-bp Cy3-labeled F1 dsDNAs to coverslips; the high-affinity F1 Fis binding sequence has been well-characterized thermodynamically and structurally (21). Although Fis is able to bind to a core 21-bp region of this site (21), additional contacts over the 27-bp window stabilize binding (29, 30), and shorter DNA oligos show weaker binding properties (21, 25, 30), indicating 27 bp to be the complete binding site length.

We determined the off rate of gfpFis in protein-free 100 mM NaCl buffer by measuring the number of gfpFis molecules that remain bound to F1 DNAs as a function of time (Fig. 1*A*). We observed a high degree of colocalization (up to ∼85%) between signals in the gfpFis and DNA channels (Fig. 1*B*), which ensures that the GFP signals that we retain for analysis correspond to Fis dimers bound to DNA. The decay curves fit well to single exponential decays of the form $\exp(-t/\tau_{off})$; a sample decay curve is shown in Fig. 1*A*. In competitor-free buffer, Fis remains stably bound for a long period ($\tau_{off} = 180 \pm 40$ min; three replicate experiments), giving a spontaneous off rate of $k_o = \tau_{off}^{-1} = (9 \pm 2) \times 10^{-5}$ s^{-1}.

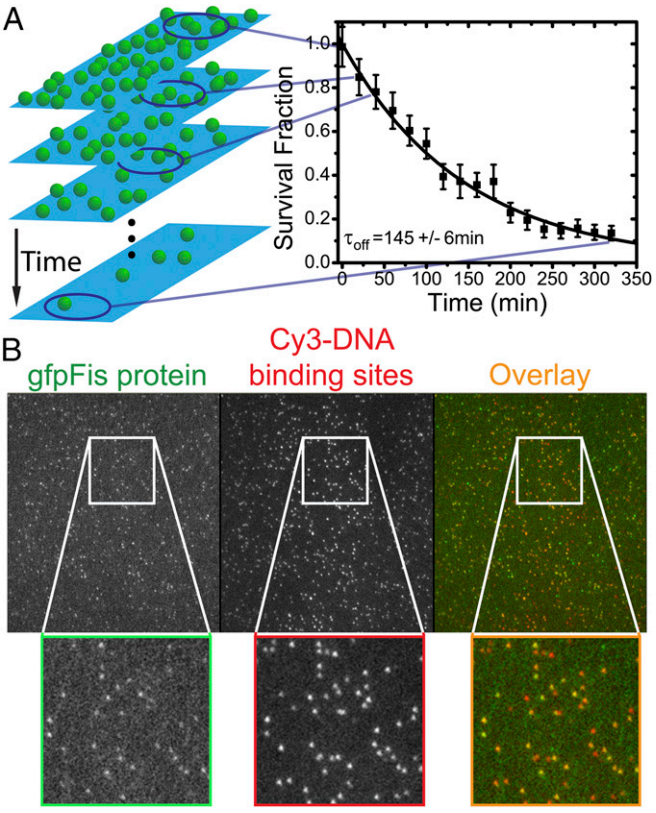

Fig. 1. Off-rate measurement. (*A*) The survival fraction is measured by counting the number of fluorescent signals (green spheres in *Left*) remaining in the flow cell as a function of time and normalizing by the initial number of signals. A new region along the flow cell is used for a measurement of the survival fraction at each subsequent time point. To obtain the off rate, the survival fraction decay is fit to a single decaying exponential $\exp(-t/\tau_{off})$ (*Right*). In the example shown, $\tau_{off} = 145 \pm 6$ min, with $\chi^2/\nu = 0.34$. *SI Materials and Methods* has details of the survival fraction calculation. (*B*) Camera frame showing single-molecule fluorescence images in separate channels. Each panel is the full 512 × 512-pixel array (52.5 × 52.5 μm^2). *Insets* are magnified views of the regions contained in the white boxes. (*Left*) Fluorescent signals from gfpFis and (*Center*) signals from Cy3-labeled F1 DNA binding sites show (*Right*) a high degree of colocalization, indicating the specificity of gfpFis binding to F1 sequences. In *Right*, gfpFis signals are false-colored green, and Cy3–DNA signals are false-colored red. Regions where green false color overlaps with red false color appear orange, indicating colocalization. Only gfpFis signals that colocalize with Cy3–DNA signals are retained for inclusion in the measurement of survival fraction.

Fis Protein in Solution Accelerates the Off Rate of Fis from Single Binding Sites. Because previous experiments showing FD for Fis involved protein initially bound along a long extended dsDNA (13), potentially containing overlapping Fis binding sites or multiprotein clusters, we were interested in whether FD could also occur at a single F1 binding site. We first confirmed that F1 sequences only allow for the stable binding of individual gfpFis dimers by recording gfpFis signal fluorescence trajectories in protein-free buffer and constructing histograms of the number of bleaching steps (Fig. S1 *A* and *B*). We observe that the majority (≈ 94%) of trajectories bleach in one or two steps as expected for single gfpFis dimers (*SI Materials and Methods* and Fig. S1).

We next recorded a series of gfpFis decay curves measured with different concentrations of wtFis in solution (0–1,790 nM) (Fig. 2*A*). Before adding wtFis, the excess gfpFis was washed out of the flow cell. We observed that, with increasing Fis concentration, the off-rate curves decay increasingly rapidly, showing that FD of Fis does not require long segments of DNA that contain multiple binding sites. The decay curves fit well to single exponential decays, and the resulting off rate ($k_{off} = 1/\tau_{off}$, the rate constant from the exponential fit) shows an initially linear increase with protein concentration (Fig. 2*B*). However, for wtFis concentrations beyond ∼250 nM, the off rate saturates. This fact indicates the presence of a rate-limiting step in the protein dissociation pathway (25).

Fis Off Kinetics Are Described by a Simple Model with a Ternary Intermediate. Our results can be described using the kinetic scheme depicted in Eq. **S6** and Fig. S2*A* (13, 27, 31), which specifies a possible mechanism by which TFs in solution lead to FD of a TF bound to DNA. This model is based on the idea that there are thermally excited, partially dissociated states where some, but not all, DNA–protein contacts are broken. A TF fully bound to its binding site (state 0) is thermally excited into a partially bound state (state 1) that is susceptible to invasion by a TF from solution to form an unstable ternary complex (state 2). The off rate of Fis corresponds to the inverse of the mean time $\langle\tau_{off}\rangle$ for a fully bound Fis molecule to transition to a fully unbound state (state 3) by either spontaneously dissociating (transitioning directly from state 1 to state 3) or FD.

A calculation (*SI Materials and Methods* and Eq. **S10**) of the mean time to dissociation under this scheme gives the following form for the off rate (25):

$$k_{off} = \frac{c + D}{Ac + B}, \qquad [1]$$

where c is [wtFis]. The constants A, B, and D are combinations of the microscopic rate constants from the kinetic model. By using Eq. **1** to fit the data (Fig. 2*B*), we determine $k_{exch} = 1/B - DA/B^2 = (1.0 \pm 0.2) \times 10^4$ M^{-1} s^{-1}. The saturated rate at high wtFis concentration is $k_{sat} = 1/A = (8.1 \pm 1.5) \times 10^{-3}$ s^{-1}, which is nearly 100-fold larger than the spontaneous dissociation rate $k_o = (9 \pm 2) \times 10^{-5}$ s^{-1}. Qualitatively, our observation that the off rate of Fis from DNA is accelerated by Fis proteins in solution and quantitatively, the approximate exchange rate are both in agreement with previous single-DNA protein competition experiments (13) as well as experiments showing FD for Fis bound to the *E. coli* nucleoid (14). Our results show that FD does not necessarily require long stretches of DNA that contain overlapping binding sites (32) or clusters of proteins.

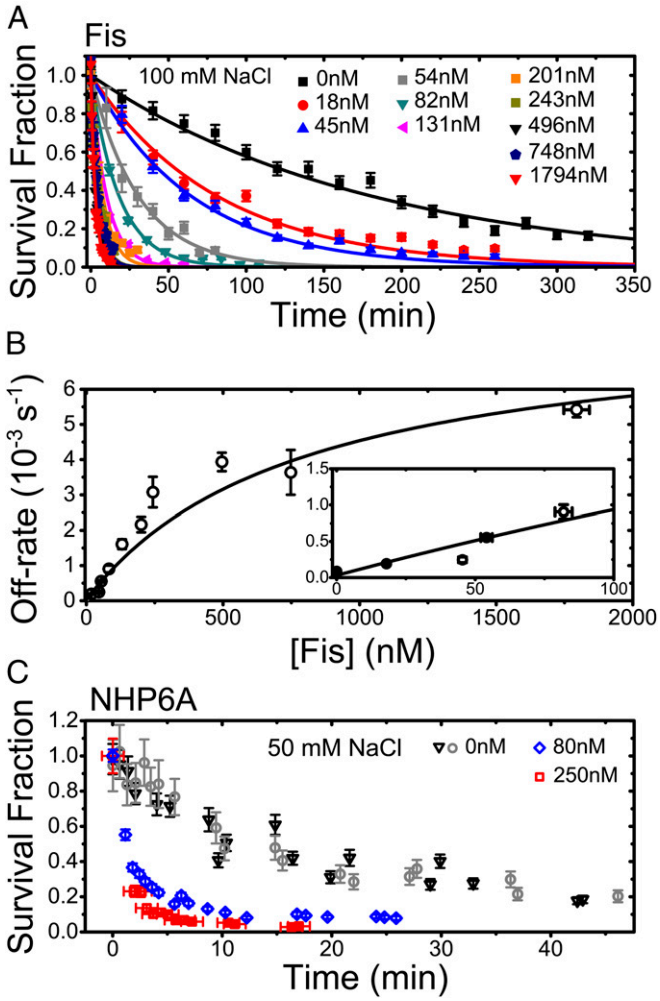

Fig. 2. TF dissociation measurements from single binding sites. (*A*) Sample survival fraction time course measurements (symbols) for gfpFis at each concentration of wtFis in solution that was tested. Error bars are estimates of the statistical uncertainty in the data points from various sources (*SI Materials and Methods*). At each concentration, the early portion of the survival fraction decay is well-fit to a single exponential decay to obtain the off rate (curves; typically $\chi^2/\nu \sim 1$). (*B*) Off rate vs. concentration of wtFis in solution. Vertical error bars are a weighted SD of two to four measurements, except for the measurement at 54 nM, which contains a single measurement (*SI Materials and Methods*). Sizes of the horizontal error bars are smaller than the symbols (except for data point at 1,794 nM) and represent statistical error in [wtFis]. (*Inset*) Low-concentration behavior. Solid curve is a fit to Eq. **1**. The exchange rate k_{exch} and saturation rate k_{sat} are estimated from the fit and given by $B^{-1} - DA/B^2 = (1.0 \pm 0.2) \times 10^4$ M^{-1} s^{-1} and $A^{-1} = (8.1 \pm 1.5) \times 10^{-3}$ s^{-1}, respectively; D is within 0–8 nM, and $\chi^2/\nu \approx 9$. Errors are scaled by $\sqrt{\chi^2/\nu}$. If the ratio D/B is fixed to the measured value [$D/B = k_o = (9 \pm 2) \times 10^{-5}$ s^{-1}], B and A change by 16.9 and 7.6%, respectively, which are within error. (*C*) NHP6A survival fraction time courses showing that NHP6Agfp also displays FD from single binding sites using wtNHP6A as a competitor. Experiments performed in protein-free 50 mM NaCl buffer are shown for two duplicate trials (gray and black symbols). Vertical error bars are estimated as in *A*. The datasets corresponding to 80 and 250 nM [wtNHP6A] are normalized to the number of signals measured after the survival fraction has already decayed by reincubating the flow cell with NHP6Agfp and counting the number of signals under protein-free buffer conditions.

NHP6A Also Displays FD from SRY Binding Sites. To determine whether dimeric structure (e.g., Fis) is required for FD, we measured survival probability decay curves of NHP6A, a monomeric TF in yeast that consists of a single HMGB box domain (9), using the same approach that we used for Fis. For an NHP6A binding site, we used a short Cy3-labeled dsDNA segment containing the recognition sequence for the SRY protein, because an NMR solution structure for the SRY DNA–NHP6A complex has been determined (9). Survival probability curves of NHP6Agfp fusions, measured in 50 mM NaCl buffer that includes 80 or 250 nM wtNHP6A, showed faster decays than those in protein-free buffer (Fig. 2*C*). Our results with monomeric NHP6A, which has a different structure and binding mode than dimeric Fis, show the generality of FD.

Salt Dependence of Spontaneous Off Rate Is Strong; Salt Dependence of FD Is Weak. Returning to the case of Fis, we measured the univalent salt concentration dependence of the off rate. We reasoned that this would provide a molecular-level probe of the kinetic pathways involved in FD. We first measured the salt dependence of the off rate in protein-free buffer (Fig. 3 *A* and *C*) at several salt concentrations, c_S, in the range of 75–250 mM NaCl, and we observed a strong salt dependence: the off rate fits to a power law of the form $k_{off} = a c_S^M$, with exponent $M = 2.6 \pm 0.3$. The overall spontaneous dissociation pathway ($0 \rightarrow 1 \rightarrow 3$ in Fig. S2*A*) is, therefore, strongly salt-dependent.

To probe the [wtFis]-dependent FD pathway, we next measured the off rate with 243 ± 6 nM wtFis in solution at several c_S values in the range of 20–300 mM NaCl (Fig. 3 *B* and *C*) [this wtFis concentration is roughly halfway up the FD off-rate curve in Fig. 2*B* and also likely comparable with the free wtFis concentration found in vivo (14)]. The observed salt dependence is weak (Fig. 3*C*), suggesting that either the protein-dependent pathway does not depend on salt concentration or it is rate-limited by a salt-independent step. This observation suggests fitting the 243 nM data to the combined power-law form:

$$k_{off} = a\, c_S^M + b\, c_S^m c, \qquad [2]$$

where a and M are fixed to the values obtained by fitting the protein-free data. The fits to the 243 nM data (Fig. 3*C*) can accommodate a power-law exponent no larger than $m \approx 0.25$, with the best fit given by $m = 0$ (i.e., no salt dependence at all).

It is well-established that the dissociation constant for many protein–DNA interactions has a power-law dependence on univalent salt concentration, c_S, leading to $\log K_D$ vs. $\log c_S$ being linear (33, 34):

$$\frac{\partial \log K_D}{\partial \log c_S} = n, \qquad [3]$$

where the slope n is proportional to the number of positive counterions released from the DNA molecule or equivalently, the number of contacts formed between the protein and the DNA when the protein binds (35). This relation motivates the use of power laws in Eq. **2** to fit the salt dependence of the off rate in Fig. 2*C*, because $k_{off} = \gamma K_D$ for a simple bimolecular reaction. It should be noted that the partial dissociation model makes the prediction (which we have confirmed here) (Fig. 3*C*) that, over some range of c_S, which depends on the protein concentration, the salt dependence of the off rate is weaker when proteins are in solution (explained in *SI Materials and Methods* and depicted in Fig. S2*B*). These results suggest that the number of counterions released in forming a ternary complex during FD is a small fraction of the number of counterions that condense on the binding site when Fis is released during spontaneous dissociation.

Partial Unbinding Model Simultaneously Explains c_s and c Dependence. We sought to generalize Eq. **1** to account for the observed salt dependence. We formulated a model (Fig. 4*A* and Fig. S3) that incorporates the effects of DNA-bound counterions on the free

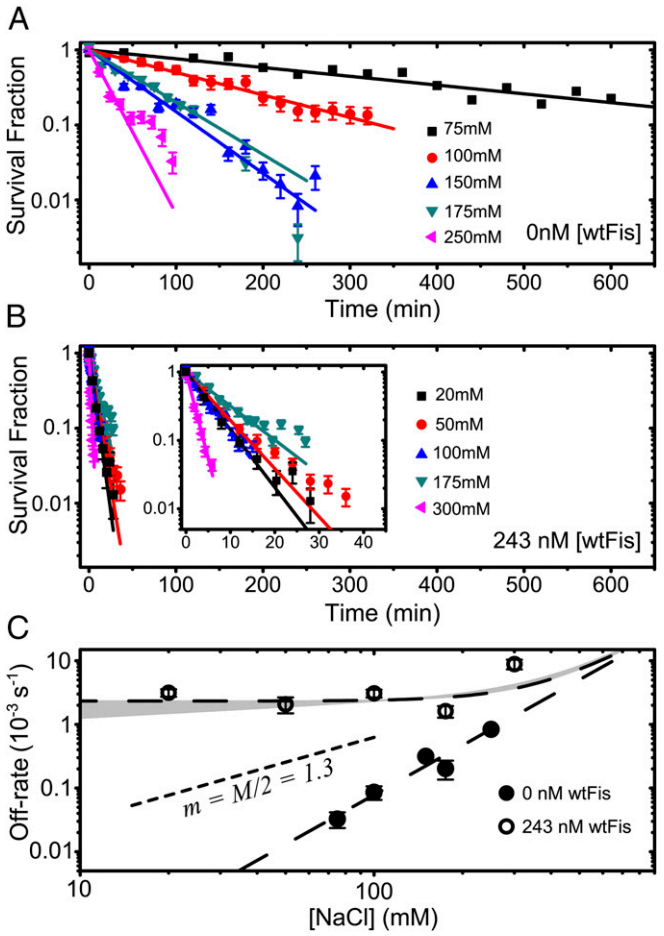

Fig. 3. Salt dependence of off rate. (*A*) gfpFis decay curves measured in protein-free buffer at multiple NaCl concentrations. (*B*) gfpFis decay curves measured in buffer containing 243 nM [wtFis] at multiple NaCl concentrations. (*Inset*) Same data shown on a zoomed in scale to show detail. In both *A* and *B*, the early portions of the survival fraction curves are fit to a single exponential decay to obtain the dissociation rate, and the error bars are estimated just like in Fig. 2*A*. (*C*) Off rate of gfpFis as a function of NaCl concentration in protein-free buffer (black symbols) and buffer containing 243 nM [wtFis] (white symbols). Error bars are estimated as in Fig. 2*B*. Long dashed curves are power-law fits. The protein-free off rate is fit to a single power law ($k_{off} = ac_S^M$), giving $M = 2.6 \pm 0.3$. The 243 nM off rate is fit to a sum of power laws ($k_{off} = ac_S^M + bc_S^m c$) (Eq. **2**), with M and a fixed to the values obtained by fitting the protein-free data. The gray band is a range of fits to the 243 nM data obtained by allowing joint variation in m and b while still allowing for a plausible fit. In these fits, m ranged from 0 to 0.25, beyond which the slope of the power law did not allow for reasonable agreement with the data. A single power-law exponent equal to $M/2$ is shown for comparison (short dashed curve).

energies involved in the kinetic steps along both dissociation pathways. The model also allows for asymmetric unbinding of the protein from the DNA. We used the exact analytical calculation (above) of the mean time $\langle \tau_{off} \rangle$ (Eq. **1** and Eq. **S10**) for a protein to dissociate from the DNA binding site in terms of the microscopic rate constants k_{ij} (arrows in Fig. 4*A*) and the protein concentration, c = [wtFis], in solution. Using detailed balance, the salt dependencies of the set of k_{ij} are included, which results in a model for the off rate, $k_{off} = \langle \tau_{off} \rangle^{-1}$, in terms of the physical parameters of the model, the protein concentration, and the ionic strength (see *SI Materials and Methods* and Fig. S3 for a detailed derivation). The incoming wtFis molecule forms a ternary complex by binding to the partially exposed binding site, destabilizing the binding of the original gfpFis molecule, and blocking its return to state 1. In our model, this transition leads to the dissociation of both the initially bound gfpFis and the incoming wtFis molecules (arrow k_{23} in Fig. 4*A*); however, it is also possible that the wtFis molecule replaces the original molecule (arrow k_{20^*} in Fig. 4*A*).

We performed a global fit to the c and c_s dependences of the off rate using this model (*SI Materials and Methods* has fitting details). Because the large number of parameters made fitting impossible, we fixed the bimolecular on-rate constant γ by direct measurement (*SI Materials and Methods* and Fig. S4) to reduce the number of free parameters. We made the simplifying assumption that the measured on-rate constant γ_{meas} corresponds to the rate γ for Fis to bind to sites that already contain partially bound Fis molecules in state 1. However, we expect that γ as

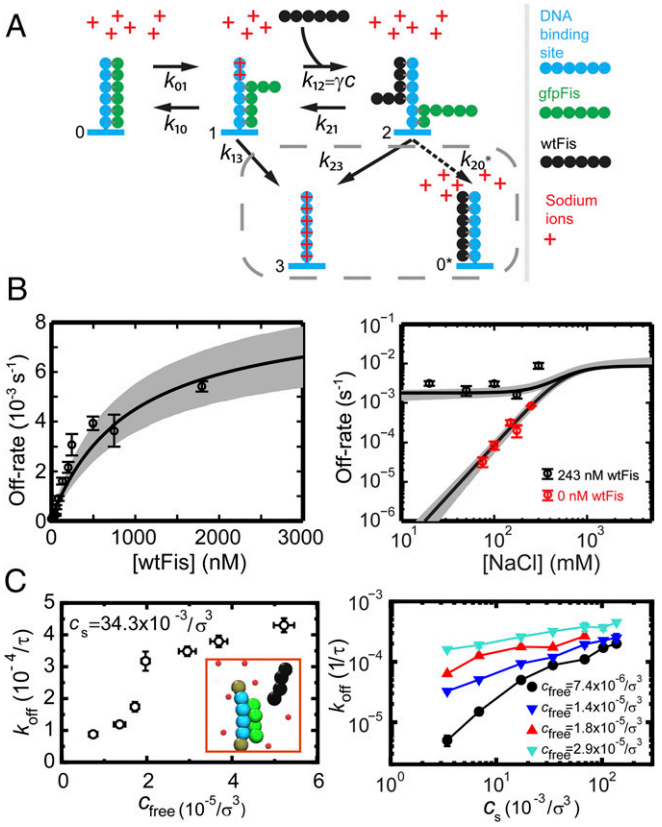

Fig. 4. Global fit to kinetic model and simulations. (*A*) Schematic representation of a kinetic model of FD. Schematic depicts the multivalency of Fis–DNA interactions by drawing Fis as a multipartite object. However, this sketch should not be interpreted as Fis taking a linear form. The model explicitly includes positive Na^+ ions in solution, which can condense on DNA and compete with binding locations on Fis for contacts to the DNA. Going from state 1 to state 2, the original TF (green) is shown with fewer contacts to the DNA to depict the possibility that the competitor could destabilize the binding of the original TF. The gray box encircles the two possible final states of the ternary complex; however, this study considers the left-pointing solid arrow. *SI Materials and Methods* has a detailed derivation of the mean reaction time, including the salt and protein concentration dependence with this kinetic model. (*B*) [wtFis] (*Left*) and [NaCl] (*Right*) dependence measurements of the off rate are globally fit to extended kinetic model (solid curves). Bimolecular on-rate constant $\gamma = 1.04 \pm 0.19 \times 10^8$ M^{-1} s^{-1} is fixed by experiment (*SI Materials and Methods*) in the fitting. Gray bands represent 68.3% confidence intervals of the fit (*SI Materials and Methods*). (*C*) Coarse-grained simulations correspond to an extended kinetic model where protein and DNA molecules are represented by chains of reactive beads as illustrated in *Inset* (*SI Materials and Methods*). (*Left*) Protein concentration dependence of the off rate obtained from the simulations. Off rate is plotted in units of the inverse self-diffusion time τ of a bead (*SI Materials and Methods*). (*Right*) Salt concentration dependence of the off rate at multiple protein concentrations.

defined in the model is somewhat less than γ_{meas}, because it is measured on initially empty binding sites. A smaller γ will lead to fitted values for the microscopic kinetic constants that differ from those that come from our fit to the model (Table 1). However, the fit is well-constrained by the data and is shown in Fig. 4*B*. Furthermore, the kinetic rate k_{01} is well-constrained by the data, even before γ is fixed. All of the kinetic rates of the model except k_{23}, which has a broad distribution (Table 1), are well-constrained by the data. However, it is clear that k_{23} is large compared with k_{01}, and therefore, k_{01} is rate-limiting for the competitor-dependent pathway. Despite the fact that the microscopic rate constants (except for k_{01}) that come from the fit cannot all be obtained accurately, the model is able to simultaneously capture the weak (essentially absent) salt dependence of the 243 nM data between 20 and 175 mM NaCl, the strong salt dependence of the protein-free measurements, and the saturation of the off rate at high protein concentrations. Therefore, our findings support partial unbinding of Fis as the molecular mechanism of FD.

Coarse-Grained Simulations Validate Multivalent Partial Unbinding Model. To judge the applicability of the multivalent partial unbinding model, we performed coarse-grained MD simulations (Fig. 4*C* and *SI Materials and Methods*) designed to mimic features of our experiment and our revised model by a generic bead spring model (*Inset* in Fig. 4*C*, *Left* and Fig. S5). Specifically, the simulations explicitly included multivalent structure in the DNA binding sites and competitor protein molecules and in addition, explicitly included positive charges in solution that could serve as counterions to compete for binding with positively charged protein molecules. The individual DNA binding sites are each represented by a chain of four negatively charged beads, and the proteins are represented by chains of four positively charged beads. All beads interact via long- and short-range Coulomb interactions. The steric interactions between beads are taken into account by repulsive excluded volume potentials; attractive interactions are only between the binding site and proteins (*SI Materials and Methods*). We note that, although we define our model via interaction potentials, it is possible to directly implement chemical reaction rates instead (36).

The simulations show a strongly accelerated off rate of prebound protein when competitor proteins are introduced (Fig. 4*C*, *Left*), qualitatively in accord with both our experimental data and our analytical model. The simulations also display the saturation of off rate at large competitor concentrations (Fig. 4*C*, *Left* and Fig. S6) seen experimentally and in the analytical model. Finally, the simulations also produce a strong salt dependence in the absence of protein in solution (black curve in Fig. 4*C*, *Right* and Fig. S6) and weak salt dependence at high protein concentrations, again qualitatively in accord with experiment and the analytical model.

It is important to note that, for reasons of computational power, the MD simulations must be done for weaker and consequently, shorter-lived protein–DNA interactions than occur for Fis or NHP6A in our experiments. In the simulations, the length scale σ, which corresponds to the size of a bead and is set by the requirement that the electrostatic energy between two beads in surface contact has to be equal to k_BT, is ~0.7 nm, making $1/\sigma^3 \sim 5$ M and $1/\tau \sim 4 \times 10^9$ s^{-1}, where τ is the self-diffusion time of a bead, k_B is Boltzmann's constant, and T is the absolute temperature, indicating that comparison of MD and experiment can be only qualitative. However, the MD results indicate that similar FD effects can be expected for biomolecule interactions that are far weaker and shorter-lived than we can study with our current time resolution.

Table 1. Microscopic rate constants obtained from global fitting with the FD model

Rate constant	Constraints from fitting or measurement*
k_{01}	$8.7^{+1.4}_{-1.4} \times 10^{-3}$ s^{-1}
k_{10}	90^{+30}_{-20} s^{-1}
k_{13}	$900^{+310}_{-270} \times 10^{-3}$ s^{-1}
k_{23}	$4^{+24}_{-2} \times 10^6$ s^{-1}
k_{21}†	$k_{21} \le k_{23}/600$ $k_{21} \sim k_{23}/10^{9\pm1}$
γ	$1.04^{+0.19}_{-0.19} \times 10^8$ M^{-1} s^{-1}
n_{01}	0–0.25
n_{13}	$2.55^{+0.30}_{-0.25}$

Rate constants are referenced to their values at 100 mM NaCl; γ, n_{01}, and n_{13} are not fitted parameters, but they are instead measured values with distributions that are imposed on the fit in Fig. 4*B*.

*Except for k_{21}, all constraints are statistical 68% confidence intervals. Quoted values are those that minimize χ^2 with γ, n_{01}, and n_{13} fixed to their measured most probable values. Additional systematic uncertainty in the kinetic rates comes from γ being known only up to an overall unknown factor. Note that the combination of $n_{01} + n_{13}$ and not n_{13} directly is measured. Uncertainty on n_{13} is, therefore, estimated from direct measurement of n_{01} and by simulating errors on n_{13} given the experimental errors on n_{01} and $M = n_{01} + n_{13}$.

†Although k_{21} was not a fitting parameter in the final fitting function S21 (k_{21} is ignored compared with k_{23} in Eq. S19), placing constraints on it was possible by performing fits using an equation derived from Eq. S19. The upper limit on k_{21} is found by fixing α_{21} to $\alpha_{23}(100\text{ mM})^{n_{13}-n_{01}}/N$ and finding the minimum value of N that allows consistency with the data.

Discussion

Kinetic Survival Fraction Measurements Are Well-Suited for Studying the Molecular Basis of FD. In this study, we have shown that the TF Fis undergoes FD from single binding sites formed from short DNAs. Previous single-DNA protein competition experiments on Fis showed FD on extended 48.5-kb DNA molecules (13). However, interpretation of these experiments is complicated by the fact that there are multiple binding sites of varying affinity on long DNA molecules, which can lead to nonexponential decays of survival probability (27). Moreover, binding sites that overlap could assist FD (32) or allow for other types of cooperative dissociation events. This possibility initially raised the question of whether FD with Fis requires protein clusters, the action of overlapping binding sites, or whether the competitor acts by sliding along adjacent DNA segments. Because our study uses a single binding site with a single binding strength, our results indicate that FD with Fis does not require long DNAs or cooperative binding effects, and this conclusion is further supported by our observations of single exponential decays (Figs. 1*A*, 2*A*, and 3 *A* and *B*).

Because we can readily measure slow off rates over a large dynamic range of TF concentrations (Fig. 2), our method of measuring the survival fraction is able to observe FD of very high-affinity TFs ($K_D \approx 1$ pM for Fis–F1 interaction at low [wtFis] in our experiment). We are able to observe saturation of the off rate, which until now, has only been observed in DNA competition experiments (25). In contrast, detection of FD on high-affinity TFs, displaying slow off rates, might be missed using methods that rely on the collection of on/off binding events [e.g., single-molecule Förster resonance energy transfer (smFRET)] because of fluorophore bleaching hampering long observation times and limitations on the concentration of competitor that can be used (high competitor concentrations would lead to intervals between binding events that are shorter than the time resolution). These considerations likely explain why FD of NHP6A was not seen using smFRET in a previous study (37).

Microscopic Picture of FD with Fis. By fitting our results to an exactly solvable theoretical model including salt effects, we developed a microscopic picture of FD (Fig. 4*A*). At high wtFis concentration, the off rate saturates at $k_{sat} = k_{01}k_{23}/(k_{01} + k_{23}) \approx k_{01}$ (from fitting

with the model, we find $k_{23} \gg k_{01}$), indicating that the rate-limiting step along the FD pathway is the rate at which a fully bound protein is thermally excited into a partially bound state, thereby exposing the binding site to invasion by a competitor. There is a waiting time of ~ 2 min (given by $1/k_{sat}$) for a bound Fis molecule to become susceptible to invasion, after which the formed ternary complex quickly leads to dissociation. The fact that k_{23} is large compared with k_{13} shows that the original TF is more strongly bound in the partially dissociated state (state 1) than in the ternary complex (state 2). The transition from state 1 to state 3 is essential for the model to capture the spontaneous dissociation of Fis at low competitor concentration.

The nearly absent salt dependence of the FD pathway reflects the weak salt dependence of the rate-limiting kinetic step from states $0 \rightarrow 1$ (Figs. 3*C* and 4*A*) and suggests that few protein–DNA contacts are broken along the pathway leading to a ternary complex. It also indicates that, during FD, the two Fis molecules are within one screening length relative to each other, so that the total number of protein–DNA contacts is approximately conserved by the formation of the ternary complex. Although a rigorous quantitative understanding of the microscopic picture of FD with Fis is limited by our knowledge of the bimolecular on rate γ, our analytic model qualitatively describes our data remarkably well.

Additionally, we note that DNA near the boundaries of the 27-bp binding site may well be involved in FD, and thus, additional single-molecule studies of slightly shorter or longer DNA oligos or different flanking sequences might be useful in further understanding Fis–F1 FD. It is also unclear the degree to which protein conformational fluctuations play a role in FD. Although relatively unstructured peptides have a plausible mechanism, such as in the case of, for example, polymerase processivity clamp interactions (38), it remains to be understood how fluctuations of more stably folded proteins, such as Fis or NHP6A, allow FD to occur. Intriguingly, there is a hint in the data of a more complex (sigmoidal) shape to the rate-concentration curve (Fig. 2*B*), which may be indicative of multiple intermediate states along the FD pathway (24). MD simulations may be able to provide some hints of dynamical mechanism (20), although accessing the very long timescales associated with FD of Fis will be extremely challenging, even with a coarse-grained model.

A previous study has described how competitors in solution can accelerate dissociation of molecular complexes by occluding rapid rebinding events and shown accelerated DNA duplex dissociation by this mechanism (39). However, the concentration scale, c, for this effect to occur is given by $c \approx 1/\delta^3$, where δ is the size of the reaction volume, which in our case, is of the order $\delta \sim 10$ nm. This argument would suggest a concentration scale of $c \approx 2$ mM for FD, but we already see a significant enhancement in off rate at 20 nM. In addition, for a binder and target that are roughly the same size, inhibition of rebinding typically leads to only an approximately 2-fold effect, because the expected number of rebinding events is of order 1, but we observe a nearly 100-fold effect. Finally, it is hard to explain the observed weak salt dependence of the protein-dependent pathway using this type of model, because the intermediate state involves a fully unbound protein. Taken together, our results argue against a rapid rebinding model and support the formation of a ternary complex as the mechanism underlying the concentration-dependent off rate of Fis. This conclusion is further supported by recent computational studies exploring the energy landscape of Fis binding that show the existence of a Fis–DNA–Fis ternary complex (20) and our simulations showing that FD via a ternary complex mechanism qualitatively recapitulates our experimental observations (Fig. 4*C*).

Generic Nature of FD. We expect that FD should occur for any TF–DNA interaction that involves multiple contacts between the TF and DNA as long as the TF–DNA complex can partially unbind and expose the binding site to invasion by competitors. Our observation of FD of a monomeric protein, NHP6A, supports this assertion (Fig. 2*C*). We also note that we have observed heterotypic FD (Fis-driven dissociation of NHP6A) (Fig. S7) (13), which is indicative of a rather generic mechanism.

FD is unmistakable in experiments like ours and those of others (11–13, 15, 16, 18), which have single-molecule dynamics that are observable at $\approx$ 1-s timescales because of strong protein–DNA interactions ($K_D \leq 100$ nM). However, FD is likely a general effect, controlling the unbinding kinetics of proteins with micromolar affinities, and typical single-molecule experiments with >10 -ms time resolutions are unable to observe these submillisecond dynamics. Our MD simulations, which by necessity, use weak binding sites, support this assertion, exhibiting FD at high competitor concentrations. This observation suggests that FD could occur in vivo for typical TFs that bind much more weakly to DNA than Fis. Furthermore, although a high concentration of an individual type of weakly binding TF may not be present in vivo, high concentrations of other proteins can be expected, and it has already been seen that competitor TFs of one type can cause FD of another type (13, 14). Therefore, it is reasonable to expect that FD could be an important mechanism for buffering the effective K_D and assisting in the local exchange of a large class of TFs from chromatin in the nucleus.

Physiological Relevance of FD. In *E. coli*, it is observed that Fis is largely replaced by other nucleoid-associated proteins during slow bacterial growth (40). Our observation that competitors accelerate the dissociation of Fis from 1 pM affinity F1 sites suggests that FD plays an important role in this exchange and possibly serves as a mechanism to modulate the occupancy of strong Fis binding sites at high protein concentrations in vivo. Indeed, it has been observed that Fis binding lifetimes on the nucleoid are faster in vivo (where free Fis concentrations are at least several hundred nanomolar) than they are on isolated nucleoids (14, 41), which suggests FD driven by a cytoplasmic concentration of Fis (and other DNA binding proteins) in the few hundred nanomolar range.

Our results suggest that FD could have a profound effect on the dynamics of biological processes that depend on the binding of TFs in vivo. Cellular gene expression profiles and protein concentration levels occurring in complex regulatory networks should be affected by FD through its ability to shorten the residency time of a wide class of TFs that control these networks. FD may also play a role in regulating the dynamics of chromatin structure by facilitating the exchange of TFs with other regulatory proteins, such as histones, nucleosomes, and remodelers from chromatin (6, 8, 42). In particular, FD could be a mechanism for regulating the ability of high-affinity TFs to switch transcription on and off and possibly facilitates TF mobility along the genome. Furthermore, our simulations suggest that FD should accelerate removal of proteins that bind DNA far more weakly than Fis (Fig. 4*C*) at timescales far shorter than our current single-molecule experiment can access. In conclusion, FD of TFs may be an important general effect to take into account in systems biology simulations that model gene expression in cells.

Materials and Methods

Single-molecule experiments were carried out using Cy3- and biotin-labeled 27-bp dsDNA oligomers, which were attached to the interior of a flow cell via streptavidin and biotin-PEG. Proteins were introduced via flow, including gfp-labeled proteins. The DNAs and gfp-labeled proteins were imaged using total internal reflection fluorescence imaging, which allowed individual DNAs and proteins to be observed. Time series of protein occupation of DNAs were collected and then analyzed to obtain protein binding kinetics. Coarse-grained MD simulations were carried out using a simulation box containing 100 sparsely placed surface-grafted semiflexible DNA chains (binding sites), an equal number of protein (flexible) chains initially bound onto the DNA chains, a prescribed number of initially unbound proteins, counterions for protein and DNA chains, and a prescribed number of monovalent salt ions. The DNA and proteins are modeled by a coarse-grained bead spring model

with both short- and long-range electrostatic interactions. Additional details of single-molecule and simulation methods may be found in *SI Materials and Methods*.

All data, documentation, and code used in analysis will be made available on request to M.O.d.l.C. and J.F.M.

ACKNOWLEDGMENTS. Work at Northwestern University was supported by NIH Grants R01-GM105847 and U54-CA193419 (CR-PS-OC), a subcontract to NIH Grant U54-DK107980, and National Science Foundation Grants MCB-1022117, DMR-1611076, and DMR-1206868. Work at the University of California, Los Angeles, was supported by NIH Grant GM038509.

1. Christmann M, Kaina B (2013) Transcriptional regulation of human DNA repair genes following genotoxic stress: Trigger mechanisms, inducible responses and genotoxic adaptation. *Nucleic Acids Res* 41:8403–8420.
2. Dominguez-Sola D, et al. (2007) Non-transcriptional control of DNA replication by c-Myc. *Nature* 448:445–451.
3. Ganapathi M, et al. (2011) Extensive role of the general regulatory factors, Abf1 and Rap1, in determining genome-wide chromatin structure in budding yeast. *Nucleic Acids Res* 39:2032–2044.
4. Guerra RF, Imperadori L, Mantovani R, Dunlap DD, Finzi L (2007) DNA compaction by the nuclear factor-Y. *Biophys J* 93:176–182.
5. Ong CT, Corces VG (2014) CTCF: An architectural protein bridging genome topology and function. *Nat Rev Genet* 15:234–246.
6. Ramachandran S, Henikoff S (2016) Transcriptional regulators compete with nucleosomes post-replication. *Cell* 165:580–592.
7. Sanyal A, Lajoie BR, Jain G, Dekker J (2012) The long-range interaction landscape of gene promoters. *Nature* 489:109–113.
8. Voss TC, Hager GL (2014) Dynamic regulation of transcriptional states by chromatin and transcription factors. *Nat Rev Genet* 15:69–81.
9. Masse JE, et al. (2002) The S. cerevisiae architectural HMGB protein NHP6A complexed with DNA: DNA and protein conformational changes upon binding. *J Mol Biol* 323:263–284.
10. Alverdi V, Hetrick B, Joseph S, Komives EA (2014) Direct observation of a transient ternary complex during IκBα-mediated dissociation of NF-κB from DNA. *Proc Natl Acad Sci USA* 111:225–230.
11. Chen TY, et al. (2015) Concentration- and chromosome-organization-dependent regulator unbinding from DNA for transcription regulation in living cells. *Nat Commun* 6:7445.
12. Gibb B, et al. (2014) Concentration-dependent exchange of replication protein A on single-stranded DNA revealed by single-molecule imaging. *PLoS One* 9:e87922.
13. Graham JS, Johnson RC, Marko JF (2011) Concentration-dependent exchange accelerates turnover of proteins bound to double-stranded DNA. *Nucleic Acids Res* 39:2249–2259.
14. Hadizadeh N, Johnson RC, Marko JF (2016) Facilitated dissociation of a nucleoid protein from the bacterial chromosome. *J Bacteriol* 198:1735–1742.
15. Joshi CP, et al. (2012) Direct substitution and assisted dissociation pathways for turning off transcription by a MerR-family metalloregulator. *Proc Natl Acad Sci USA* 109:15121–15126.
16. Kilic S, Bachmann AL, Bryan LC, Fierz B (2015) Multivalency governs HP1α association dynamics with the silent chromatin state. *Nat Commun* 6:7313.
17. Kunzelmann S, Morris C, Chavda AP, Eccleston JF, Webb MR (2010) Mechanism of interaction between single-stranded DNA binding protein and DNA. *Biochemistry* 49:843–852.
18. Luo Y, North JA, Rose SD, Poirier MG (2014) Nucleosomes accelerate transcription factor dissociation. *Nucleic Acids Res* 42:3017–3027.
19. Potoyan DA, Zheng W, Komives EA, Wolynes PG (2016) Molecular stripping in the NF-κB/IκB/DNA genetic regulatory network. *Proc Natl Acad Sci USA* 113:110–115.
20. Tsai MY, Zhang B, Zheng W, Wolynes PG (October 5, 2016) Molecular mechanism of facilitated dissociation of Fis protein from DNA. *J Am Chem Soc*.
21. Stella S, Cascio D, Johnson RC (2010) The shape of the DNA minor groove directs binding by the DNA-bending protein Fis. *Genes Dev* 24:814–826.
22. Skoko D, et al. (2006) Mechanism of chromosome compaction and looping by the Escherichia coli nucleoid protein Fis. *J Mol Biol* 364:777–798.
23. Åberg C, Duderstadt KE, van Oijen AM (2016) Stability versus exchange: A paradox in DNA replication. *Nucleic Acids Res* 44:4846–4854.
24. Cocco S, Marko JF, Monasson R (2014) Stochastic ratchet mechanisms for replacement of proteins bound to DNA. *Phys Rev Lett* 112:238101.
25. Giuntoli RD, et al. (2015) DNA-segment-facilitated dissociation of Fis and NHP6A from DNA detected via single-molecule mechanical response. *J Mol Biol* 427:3123–3136.
26. Sidorova NY, Scott T, Rau DC (2013) DNA concentration-dependent dissociation of EcoRI: Direct transfer or reaction during hopping. *Biophys J* 104:1296–1303.
27. Sing CE, Olvera de la Cruz M, Marko JF (2014) Multiple-binding-site mechanism explains concentration-dependent unbinding rates of DNA-binding proteins. *Nucleic Acids Res* 42:3783–3791.
28. Dahlke K, Sing CE (2017) Facilitated dissociation kinetics of dimeric nucleoid-associated proteins follow a universal curve. *Biophys J* 112:543–551.
29. Hancock SP, Stella S, Cascio D, Johnson RC (2016) DNA sequence determinants controlling affinity, stability and shape of DNA complexes bound by the nucleoid protein Fis. *PLoS One* 11:e0150189.
30. Pan CQ, et al. (1996) Variable structures of Fis-DNA complexes determined by flanking DNA-protein contacts. *J Mol Biol* 264:675–695.
31. Marko JF (2015) Biophysics of protein-DNA interactions and chromosome organization. *Physica A* 418:126–153.
32. Chen X, Ji Z, Webber A, Sharrocks AD (2016) Genome-wide binding studies reveal DNA binding specificity mechanisms and functional interplay amongst Forkhead transcription factors. *Nucleic Acids Res* 44:1566–1578.
33. Datta K, LiCata VJ (2003) Salt dependence of DNA binding by Thermus aquaticus and Escherichia coli DNA polymerases. *J Biol Chem* 278:5694–5701.
34. Mascotti DP, Lohman TM (1990) Thermodynamic extent of counterion release upon binding oligolysines to single-stranded nucleic acids. *Proc Natl Acad Sci USA* 87:3142–3146.
35. Privalov PL, Dragan AI, Crane-Robinson C (2011) Interpreting protein/DNA interactions: Distinguishing specific from non-specific and electrostatic from non-electrostatic components. *Nucleic Acids Res* 39:2483–2491.
36. Sing CE, Alexander-Katz A (2012) Force spectroscopy of self-associating homopolymers. *Macromolecules* 45:6704–6718.
37. Coats JE, Lin Y, Rueter E, Maher LJ, 3rd, Rasnik I (2013) Single-molecule FRET analysis of DNA binding and bending by yeast HMGB protein Nhp6A. *Nucleic Acids Res* 41:1372–1381.
38. Kath JE, et al. (2016) Exchange between Escherichia coli polymerases II and III on a processivity clamp. *Nucleic Acids Res* 44:1681–1690.
39. Paramanathan T, Reeves D, Friedman LJ, Kondev J, Gelles J (2014) A general mechanism for competitor-induced dissociation of molecular complexes. *Nat Commun* 5:5207.
40. Ishihama A, et al. (2014) Intracellular concentrations of 65 species of transcription factors with known regulatory functions in Escherichia coli. *J Bacteriol* 196:2718–2727.
41. Hadizadeh Yazdi N, Guet CC, Johnson RC, Marko JF (2012) Variation of the folding and dynamics of the Escherichia coli chromosome with growth conditions. *Mol Microbiol* 86:1318–1333.
42. Misteli T, Gunjan A, Hock R, Bustin M, Brown DT (2000) Dynamic binding of histone H1 to chromatin in living cells. *Nature* 408:877–881.
43. Skoko D, Wong B, Johnson RC, Marko JF (2004) Micromechanical analysis of the binding of DNA-bending proteins HMGB1, NHP6A, and HU reveals their ability to form highly stable DNA-protein complexes. *Biochemistry* 43:13867–13874.
44. Yen YM, Roberts PM, Johnson RC (2001) Nuclear localization of the Saccharomyces cerevisiae HMG protein NHP6A occurs by a Ran-independent nonclassical pathway. *Traffic* 2:449–464.
45. Joo C, Ha T (2012) Preparing sample chambers for single-molecule FRET. *Cold Spring Harb Protoc* 2012:1104–1108.
46. Swoboda M, et al. (2012) Enzymatic oxygen scavenging for photostability without pH drop in single-molecule experiments. *ACS Nano* 6:6364–6369.
47. Chandrasekhar S (1943) Stochastic problems in physics and astronomy. *Rev Mod Phys* 15:1–89.
48. Ninio J (1987) Alternative to the steady-state method: Derivation of reaction rates from first-passage times and pathway probabilities. *Proc Natl Acad Sci USA* 84:663–667.
49. Press WH (1988) *Numerical Recipes in C: The Art of Scientific Computing* (Cambridge Univ Press, Cambridge, UK).
50. Kremer K, Grest GS (1990) Dynamics of entangled linear polymer melts: A molecular-dynamics simulation. *J Chem Phys* 92:5057–5086.
51. Plimpton S, Pollock R, Stevens M (1997) Particle-mesh ewald and rRESPA for parallel molecular dynamics simulations. *Proceedings of the Eighth SIAM Conference on Parallel Processing for Scientific Computing* (Society for Industrial and Applied Mathematics, Minneapolis).
52. Liu S, Muthukumar M (2002) Langevin dynamics simulation of counterion distribution around isolated flexible polyelectrolyte chains. *J Chem Phys* 116:9975–9982.
53. Stevens MJ (2001) Simple simulations of DNA condensation. *Biophys J* 80:130–139.
54. Plimpton S (1995) Fast parallel algorithms for short-range molecular dynamics. *J Comput Phys* 117:1–19.
55. Humphrey W, Dalke A, Schulten K (1996) VMD: Visual molecular dynamics. *J Mol Graph* 14:33–38.
56. Alberty RA, Hammes GG (1958) Application of the theory of diffusion-controlled reactions to enzyme kinetics. *J Phys Chem* 62:154–159.